25th ABCM International Congress of Mechanical Engineering
October 20-25, 2019, Uberlândia, MG, Brazil

COB-2019-1126
SIMULATION OF BOILING HEAT TRANSFER USING A HYBRID PSEUDOPOTENTIAL LATTICE BOLTZMANN METHOD

Matheus dos Santos Guzella
Luiz Eduardo Czelusniak
Vinícius Pessoa Mapelli
Luben Cabezas-Gómez
Escola de Engenharia de São Carlos – Universidade de São Paulo – Av. Trabalhador São-Carlense 400, Parque Arnold Schimidt, São Carlos - SP, 13566-590, Brazil
matheusguzella@gmail.com
luizedu.cze@gmail.com
viniciusmapelli@gmail.com
lubencg@sc.usp.br

Abstract. *In this paper, mesoscopic simulations of boiling heat transfer are performed using a Hybrid Pseudopotential Lattice Boltzmann Method. In this model, the hydrodynamic equations are solved using the Pseudopotential Lattice Boltzmann Method (Shan-Chen Model) and the energy equation is solved by the 4th order Runge-Kutta Method. The collision operator is computed from the Bhatnagar-Gross-Krook model. Two-dimensional simulation results are presented first for the nucleation of a single bubble in the center of the heated surface. Results for the nucleation, growth and departure for a single bubble are presented, whereas bubble departure diameter and release period are compared with data from the literature. Later, qualitative results of boiling heat transfer are presented and discussed. Different surface superheating degrees are considered in order to assess the numerical model. Also, different surface wettability conditions are investigated by tuning a parameter which control the solid-fluid interaction.*

Keywords: *Boiling heat transfer, Lattice Boltzmann Method, Pseudopotential*

1. INTRODUCTION

In the recent years, the Pseudopotential Lattice Boltzmann Method (LBM) has emerged as a powerful CFD tool, showing great potential and capabilities to handle complex two-phase flow phenomena. Among these two-phase flow phenomena, boiling heat transfer is very important in many industrial applications. In regard to boiling heat transfer modes, nucleate boiling has been recognized as one of the most effective, and has been used in different cooling applications, such as nuclear reactors, computer chips and micro-electronic devices. From the theoretical point of view, nucleate boiling is extremely complex, involving processes of nucleation, growth, departure and coalescence of vapor bubbles.

Several papers have been published applying the Pseudopotential LBM for the simulation of boiling heat transfer. For example, Zhang and Chen (2003) developed a hybrid Lattice Boltzmann method based on the pseudopotential model to simulate boiling heat transfer. The LBM was applied to solve the density and velocity fields and the extended Lax-Wendroff scheme for the computation of the temperature field. However, the authors disregarded the influence of pressure variation across the interface. Later, Hazi and Markus (2009) developed a method based on the pseudopotential method to simulate nucleate boiling. The authors employed two distribution functions, one for the density field and another for the temperature field. However, the authors did not adopt an actual equation of state for real gases to couple the hydrodynamic and thermal models. In this paper, the authors used an artificial equation of state.

Gong and Cheng (2012) developed an improved phase-change lattice Boltzmann method based on modification of Shan-Chen multiphase model. This new method proposed by the authors directly incorporates a non-ideal equation of state into the model. The authors solved the density, velocity and temperature fields using the LBM, considering two distribution functions. A validation of the numerical scheme was performed comparing the bubble departure diameter with Fritz correlation. A good agreement was observed. Later, the authors published studies using this phase-change LBM to evaluate surface wettability, namely Gong and Cheng (2015a) and Gong and Cheng (2015b). However, in all these studies, the energy equation did not take into account the density variation across the interface in the diffusive term. In addition, in order to solve the energy equation with the LBM, some terms need to be discretized using finite difference schemes.

Li et al. (2015) presented the first paper to analyze different boiling regimes and wettability conditions. In this research study, the authors developed an improved pseudopotential lattice Boltzmann method for the simulation of boiling heat transfer. The lattice Boltzmann method with the MRT collision operator was to simulate the fluid flow but solves the temperature field with a traditional finite-difference scheme. An improved forcing scheme was developed in order to achieve thermodynamic consistency. The numerical results were presented for different surface superheating degrees and different wettability conditions showed good agreement with theoretical results.

In this paper, the methodology proposed by Li et al. (2015) is applied for the simulation of boiling heat transfer. In this case, a hybrid pseudopotential Lattice Boltzmann Method is used to simulate boiling heat transfer. The density and velocity fields are obtained from a distribution function and the temperature field is obtained by solving the macroscopic energy conservation equation with a traditional 4th order Runge-Kutta scheme. Different from Li et al. (2015), which used the MRT collision operator, in this paper a simpler BGK approximation is considered for the collision operator. The Peng-Robinson equation of state is used to couple the hydrodynamic and the thermal models. This research paper is organized as follows. The numerical model is formulated in Section 2. Numerical simulations of nucleation, growth and departure of a single bubble are presented and discussed in the sub-section 3.1. Then, boiling heat transfer is presented and analyzed in sub-section 3.2. Finally, in Section 4 the main conclusions are presented.

2. NUMERICAL MODEL

The Lattice Boltzmann Method is based on a mesoscopic approach for the simulation of two-phase flows. Different Lattice Boltzmann models for the simulation of two-phase flows are available in the literature. In this paper, the Pseudopotential Lattice Boltzmann Method proposed by Shan and Chen (1993, 1994) is used considering the BGK operator. The discretized evolution equation for the density distribution function is given by Chen et al. (1992):

$$f_i\left(\mathbf{x}+\mathbf{c}_i\Delta t, t+\Delta t\right) = f_i\left(\mathbf{x},t\right) - \frac{1}{\tau}\left[f_i\left(\mathbf{x},t\right) - f^{eq}\right] + F_i \tag{1}$$

Where τ is the relaxation time. The local equilibrium distribution function is obtained from a low Mach number expansion of the Maxwell-Boltzmann distribution function and it is given by Eq. (2):

$$f^{eq} = w_i\rho\left[1 + \frac{\left(\mathbf{c}_i \bullet \mathbf{v}_i\right)}{c_s^2} + \frac{\left(\mathbf{c}_i \bullet \mathbf{v}_i\right)^2}{2c_s^4} - \frac{\left(\mathbf{v}_i \bullet \mathbf{v}_i\right)}{2c_s^2}\right] \tag{2}$$

For the two-dimensional numerical simulations, the D2Q9 velocity scheme is chosen. In this case, the lattice sound speed is $c_s = 1/\sqrt{3}$. A schematic representation of the velocity scheme is given in Fig. 1:

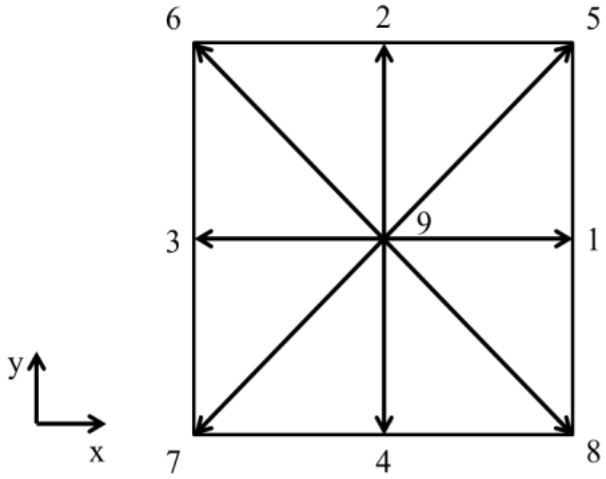

Figure 1 - Schematic representation of D2Q9 discrete velocity scheme

In this case, the lattice discrete velocities $\boldsymbol{c}_i$ and the weights w_i are given, respectively, by:

$$\mathbf{c}_i = \begin{cases} (0,0) \text{ for } i = 9 \\ (\pm 1,0),(0,\pm 1) \text{ for } i = \{1...4\} \\ (\pm 1,\pm 1) \text{ for } i = \{5...8\} \end{cases} \tag{3}$$

$$w_i = \begin{cases} 4/9 \text{ for } i = 9 \\ 1/9 \text{ for } i = \{1...4\} \\ 1/36 \text{ for } i = \{5...8\} \end{cases} \tag{4}$$

In Eq. (1), F_i is the term associated with the forces which arises in the simulation of a given problem with the LBM. For the simulation of boiling heat transfer, three different forces are considered: the interparticle force ($\boldsymbol{F}_{int}$), the adhesion force ($\boldsymbol{F}_{ads}$) and the gravity force ($\boldsymbol{F}_g$). These forces will be presented in detail.

The interparticle interaction force is responsible for phase separation in the pseudopotential model. According to Shan and Chen (1993, 1994), the computation of this interaction force is given by Eq. (5):

$$\mathbf{F}_{\text{int}} = -G\psi(\mathbf{x})\sum_i w_i^* \psi(\mathbf{x} + \mathbf{c}_i \Delta t)\mathbf{c}_i \Delta t \tag{5}$$

Where G is the interaction strength, $\psi(\boldsymbol{x})$ is the pseudopotential and w_i^* are weight parameters for the interparticle force. Shan and Chen (1993, 1994) proposed the following formulation for the pseudopotential:

$$\psi(\mathbf{x}) = \psi_0 \exp(\rho/\rho_0) \tag{6}$$

Where ψ_0 and ρ_0 are reference quantities. The weight parameters are expressed as:

$$w_i^* = \begin{cases} 0 \text{ for } i = 9 \\ 1/3 \text{ for } i = \{2,3\} \\ 1/12 \text{ for } i = \{4...8\} \end{cases} \tag{7}$$

However, the original definition of the pseudopotential presented in Eq. (6) limits the simulations to low-density ratio multiphase flows. In order to achieve high-density ratios, a non-ideal equation of state can be directly incorporated into the pseudopotential, as proposed by Yuan and Schaeffer (2006). In this case, the pseudopotential assumes the following relation:

$$\psi(\mathbf{x}) = \sqrt{\frac{2(p - \rho/3)}{|\mathbf{c}_i| G}} \tag{8}$$

In this case, G is a parameter only to ensure that the square root remains positive. In this paper, the Peng-Robinson equation of state (P-R EOS) is applied to compute the pseudopotential:

$$p = \frac{\rho RT}{1 - b\rho} - \frac{a\rho^2 \left[1 + \left(0.37464 + 1.54226\omega - 0.26992\omega^2\right)\left(1 - \sqrt{T/T_c}\right)\right]^2}{1 + 2b\rho - b^2\rho^2} \tag{9}$$

The parameters a and b in the EOS can be obtained as functions of the critical properties and can be expressed as proposed by Yuan and Schaeffer (2006) as: $a = 0.45724R^2T_c^2/p_c$, $b = 0.0778RT_c/p_c$. The acentric factor, ω, is considered as 0.344, which is the acentric factor of water.

However, with such choice for the pseudopotential, the numerical model will suffer from the lack of thermodynamic consistency. This means that the coexistence densities given by the numerical model are not consistent with the ones given by Maxwell construction. In order to address this issue, Li et al. (2012) developed an improved forcing scheme for the implementation of the interparticle force, $\boldsymbol{F}_{int}$, to ensure the thermodynamic consistency by adjusting the mechanical stability condition. This improved forcing scheme is implemented as follows:

$$F_{i,1} = w_i \Delta t \left(1 - \frac{1}{2\tau}\right)\left[\frac{(\mathbf{c}_i - \mathbf{v}')}{c_s^2} + \frac{(\mathbf{c}_i \bullet \mathbf{v}')}{c_s^4}\mathbf{c}_i\right]\mathbf{F}_{\text{int}} \tag{10}$$

Where the modified velocity is expressed as:

$$\mathbf{v}' = \mathbf{v} + \sigma \mathbf{F}_{\text{int}} / (\tau - 0.5)\psi^2 \tag{11}$$

The adhesion force, $\boldsymbol{F}_{ads}$, represents the interaction force between the solid and the fluid and is used to model the wettability (contact angle) of the solid wall. This force is implemented as presented in Li et al. (2015):

$$\mathbf{F}_{ads} = -G_s \psi(\mathbf{x}) \sum_i \frac{w_i^*}{3} s(\mathbf{x} + \mathbf{c}_i \Delta t) \mathbf{c}_i \Delta t \tag{12}$$

Where G_s is the fluid-solid interaction strength for adjusting contact angles and $s(\boldsymbol{x})$ is a function which is 1 when $\boldsymbol{x}$ is in the solid and 0 when $\boldsymbol{x}$ is in the fluid.

Finally, the gravity force is computed as:

$$\mathbf{F}_g = \mathbf{g}(\rho - \bar{\rho}) \tag{13}$$

Where $\boldsymbol{g}$ is the gravitational acceleration and $\bar{\rho}$ is the average density in the computational domain. In order to incorporate the adhesion force and gravity force, the forcing scheme proposed by Guo et al. (2002) is applied:

$$F_{i,2} = w_i \Delta t \left(1 - \frac{1}{2\tau}\right) \left[\frac{(\mathbf{c}_i - \mathbf{v})}{c_s^2} + \frac{(\mathbf{c}_i \bullet \mathbf{v})}{c_s^4} \mathbf{c}_i \right] (\mathbf{F}_{ads} + \mathbf{F}_g) \tag{14}$$

It should be noticed that the improved forcing scheme proposed by Li et al. (2015) reduces to the one proposed by Guo et al. (2002) when $\sigma=0$. The total force term in Eq (1) is given by $F_i = F_{i,1}+F_{i,2}$.

The density and velocity fields can be obtained as follows:

$$\rho = \sum_i f_i \tag{15}$$

$$\mathbf{v}_i = \frac{\sum_i \mathbf{c}_i f_i}{\rho} + \frac{(\mathbf{F}_{\text{int}} + \mathbf{F}_{ads} + \mathbf{F}_g)}{2\rho} \tag{16}$$

From Chapman-Enskog expansion, it can be shown that the Navier-Stokes equation are fully recovered. The link between the macroscopic scale and mesoscopic scale is given by kinematic viscosity, which is computed as a function of the relaxation time:

$$\nu = c_s^2 (\tau - 0.5) \tag{17}$$

The energy model is based on the discrete interface theory presented in Anderson et al. (1998). Considering the internal energy as the evolution variable at each timestep and neglecting viscous dissipation effects, the energy equation is given by:

$$\rho \left(\frac{\partial e}{\partial t} + \mathbf{v} \bullet \nabla e \right) = \nabla \bullet (k \nabla T) - p \nabla \bullet \mathbf{v} \tag{18}$$

Where k is the thermal conductivity. For a pure substance, the following equation can be obtained for the internal energy, e:

$$de = c_v dT + \frac{1}{\rho^2} \left[p - T \left(\frac{\partial p}{\partial T} \right)_\rho \right] d\rho \tag{19}$$

Where c_v is the specific heat at constant volume. Substituting Eq. (19) into Eq. (18), a temperature-based energy equation can be obtained:

$$\frac{\partial T}{\partial t} = -\mathbf{v} \bullet \nabla T + \frac{\nabla \bullet (k \nabla T)}{\rho c_v} - \frac{T}{\rho c_v} \left(\frac{\partial p}{\partial T} \right)_\rho \nabla \bullet \mathbf{v} \tag{20}$$

Equation 20 is solved using the forth-order Runge-Kutta Method (Atkinson, 1989). It should be noticed that the last term on the right-hand side couples the hydrodynamic and thermal models. Since the gravity force is computed based on the density field, the density and velocity field are first obtained and then used to compute the temperature field.

As initial condition for the hydrodynamic problem, the equilibrium distribution function, given by Eq. (2), was used to compute the density distribution function. In this case, it was assumed that the fluid velocity is known and equal to zero at all points. The density field is initialized as a liquid-vapor distribution. As boundary conditions for the hydrodynamic problem, the upper and bottom surfaces of the computational domain were modeled as walls. In this case, the no-slip condition is applied to the upper and bottom surfaces using Zou and He (1997) scheme. Hence, for the upper surface, after the streaming process, the unknown distribution functions can be obtained as follows:

$$\begin{aligned} f_4^w &= f_2^w + \frac{F_y^w}{6} \\ f_7^w &= f_5^w + \frac{1}{2}\left(f_1^w - f_3^w\right) + \frac{F_x^w}{4} + \frac{F_y^w}{6} \\ f_8^w &= f_6^w - \frac{1}{2}\left(f_1^w - f_3^w\right) - \frac{F_x^w}{4} + \frac{F_y^w}{6} \end{aligned} \tag{21}$$

The upper script ‘w’ represents the wall and F^w represents the total force which acts at the boundary. Similarly, for the bottom surface the unknown distribution function, after the streaming process, can be computed as follows:

$$\begin{aligned} f_2^w &= f_4^w - \frac{F_y^w}{6} \\ f_5^w &= f_7^w - \frac{1}{2}\left(f_1^w - f_3^w\right) - \frac{F_x^w}{4} - \frac{F_y^w}{6} \\ f_6^w &= f_8^w + \frac{1}{2}\left(f_1^w - f_3^w\right) + \frac{F_x^w}{4} - \frac{F_y^w}{6} \end{aligned} \tag{22}$$

For the lateral boundaries periodic boundary conditions are applied. It should be noticed that these kind of boundary conditions are implemented naturally from the streaming process.

All parameters are first presented in lattice units and can easily converted into SI units. For the temperature field, it is assumed that the domain is at saturation temperature. The saturation temperature is taken as a function of the critical temperature. The critical temperature can be computed using the auxiliary relations obtained from the P-R EOS, given by Eq. (9), from the parameters a, b and R. Following Li et al. (2015), these parameters are given by: $a = 3/49$, $b = 2/21$ and $R = 1$. Hence one can obtain the critical temperature as $T_c = 0.109383$. The saturation temperature is chosen as $T_{sat}=0.86T_c$. For this temperature, the equilibrium densities are $\rho_v = 0.38$ and $\rho_l = 6.5$. The kinematic viscosity of the liquid phase is taken as 0.1 and the kinematic viscosity of the vapor phase is taken as 0.5/3. Following Li et al. (2017), the relaxation time, given by Eq. (17), is computed using the kinematic viscosity of the liquid phase. The heated surface is at a higher temperature, namely T_b. The relation between this temperature and the saturation temperature is obtained from the superheating degree, $\Delta T=T_b-T_{sat}$.

To improve numerical stability for the BGK collision operator, the system is simulated at constant temperature for the first 2000 timesteps. This approach was applied by Gong and Cheng (2012). Following Li et al. (2015), the gravitational acceleration is considered after 2100 timesteps.

3. RESULTS AND DISCUSSION

In this section, numerical results of bubble nucleation, growth and departure are presented with the presented numerical model. Later, results of boiling heat transfer are presented and discussed.

3.1 Simulation of single bubble nucleation, growth and departure

In this sub-section, numerical simulations of the bubble nucleation, growth and departure using the hybrid pseudopotential Lattice Boltzmann Method are performed. A computational mesh is taken with $N_x = 151$ *and* $N_y = 300$, with N_x and N_y being the number of nodes in the horizontal and vertical. In this case, only the middle node and its immediate neighbor nodes of the bottom surface are at T_b. The others are assumed to be at saturation temperature. The

superheating degree is chosen as ΔT = 0.0427. A constant thermal diffusivity of 0.06 and a specific heat at constant volume of 5 are considered, following Li et al. (2017). The results were obtained considering $G_s=0$, which results in an equilibrium contact angle of 44.5 °. Figure 2 shows results of the nucleation, growth and departure of a bubble using the numerical model detailed in the previous section. Snapshots of the density field are presented at different timesteps in order to capture the evolution of the phenomena involved.

It can be seen that after 500 timesteps, a small nuclei appears in the bottom surface (heated surface). When the bubble is small, the pressure difference between the inside of the bubble and the liquid is higher. This growth stage is governed by inertial effects, since it is controlled by pressure difference. In this case, the thermal effects can be neglected. After 5000 timesteps, the bubble radius is higher and the pressure difference is smaller. In this case, the growth stage is governed by thermal effects. Finally, it can be seen that a vapor bubble gradually grows until the diameter reaches a critical value and departs from the heated surface. The departure occurs after approximately 15000 timesteps. After the departure of the bubble, a nuclei remains at the heated surface. It should also be noticed that the pseudopotential Lattice Boltzmann Method can naturally capture interface interactions, without the need for an interface tracking method.

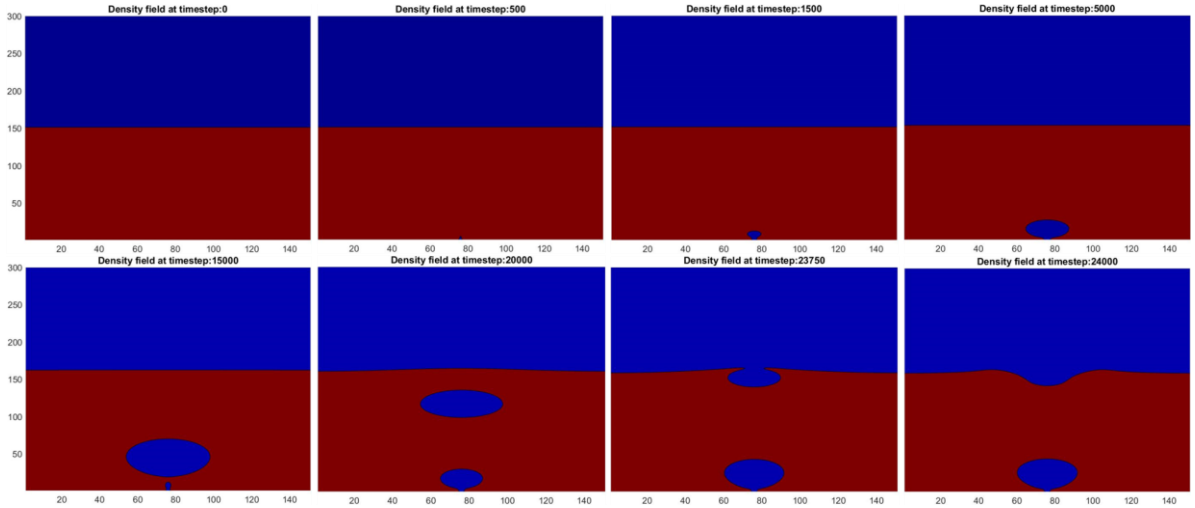

Figure 2. Nucleation of a single bubble at the center of the computational domain

Numerical results of the bubble departure diameter were obtained by varying the gravitational acceleration. In Fig. 3, the departure diameter was monitored during the simulations considering that the interface has an average density computed using liquid and vapor densities. A curve fit based on Fritz (1935) correlation is considered for comparison purposes. According to this correlation, $D_b \sim g^{-0.75}$. It can be seen from Fig. 3 that the departure diameter agrees reasonably with the curve fit based on theory.

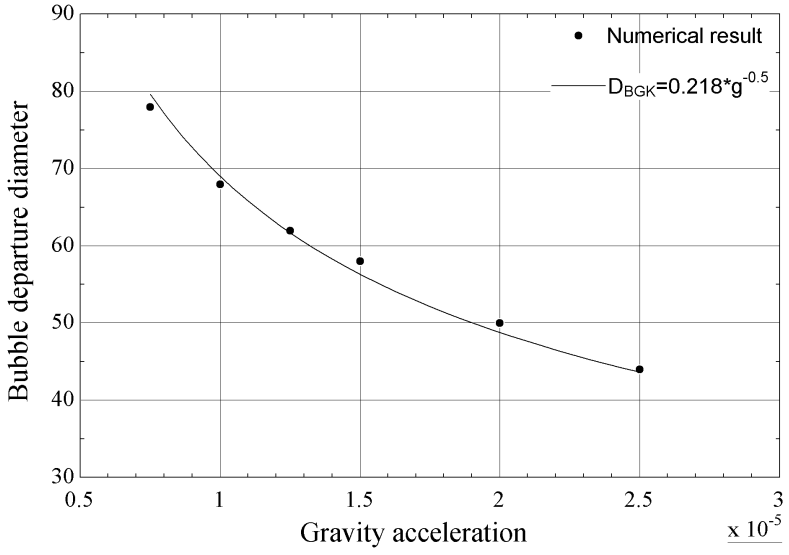

Figure 3. Bubble departure diameter as a function of gravitational acceleration

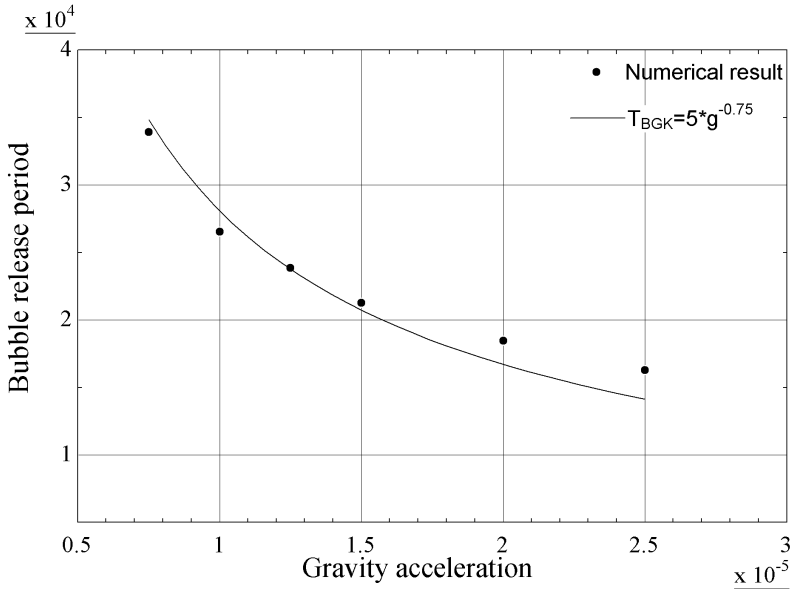

Figure 4. Bubble release period as a function of gravitational acceleration

Similarly, in Fig. 4, the bubble release period versus the gravitational acceleration was investigated. The bubble release period can be analyzed from the correlation proposed by Zuber (1963). In this study, the author showed the bubble departure period relation with gravity is $T \sim g^{-0.75}$. The results presented in Figure 4 agrees reasonably with the curve fit based on the correlation.

3.2 Simulation of boiling heat transfer

In this sub-section, boiling heat transfer is simulated using the hybrid pseudopotential Lattice Boltzmann Method. In this case, all nodes of the bottom surface are at T_b. A more refined computational mesh is considered: N_x=Ny=600. Following Li et al. (2015), the following parameters are chosen as: c_v = 6 and α = 0.028/c_v. The gravitational acceleration is taken as 2.5x10^{-5}.

Figure 5 presents numerical results of boiling heat transfer for G_s = 0. In this case, the equilibrium contact angle is about 44.5 °. The superheating degree is initially chosen as ΔT = 0.0165. When t = 10000, small vapor nuclei are formed at the heated surface. For the following stages, it can be noticed the bubble growth at the heated surface with some coalescence of the small bubbles. Later, larger bubbles are then formed and buoyancy effects lead to bubble departure from the heated surface. Finally, the rising bubbles will merge into the vapor region at the t = 35000.

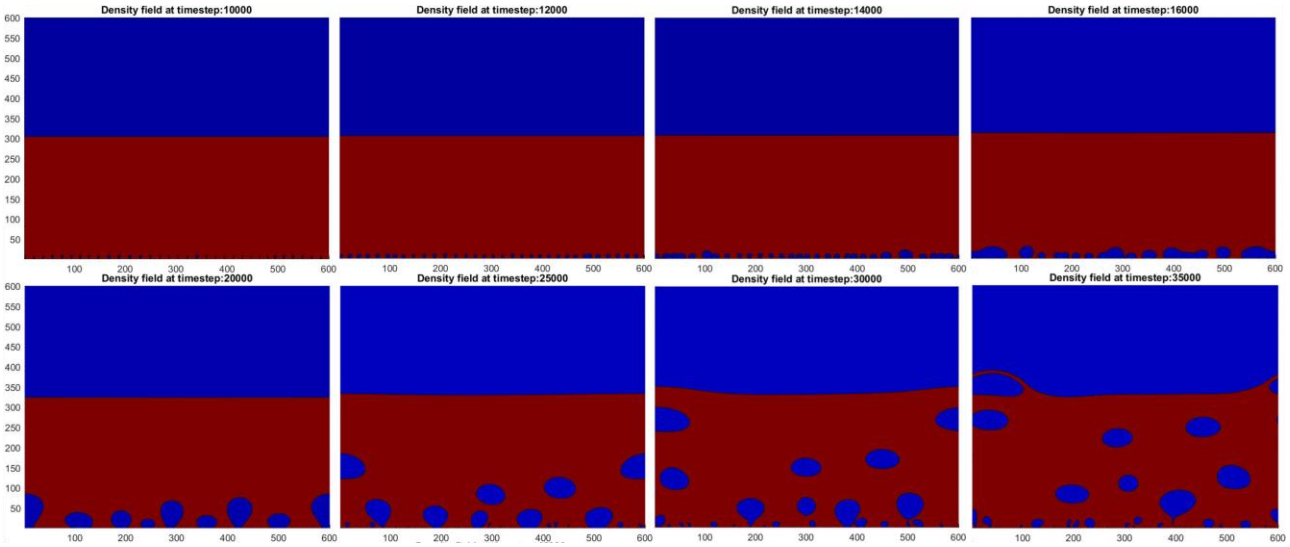

Figure 5. Snapshots of the boiling process with G_s = 0 and ΔT = 0.0165.

Now, the superheating degree is increased by 50 %, hence $\Delta T=0.0248$. Following Li et al. (2015), this higher superheating degree is imposed after 20000 timesteps. Until this timestep is reached, the superheating degree applied in the previous simulations was considered. The results are shown in Fig. 6. In this case, the vapor nuclei appears earlier, since the superheating degree is higher. Different from Fig. 5, it can be seen that a vapor film is produced near the center and small bubbles are produced on the sides. Later, this vapor film will grow and will be converted into vapor bubbles due to instabilities at the liquid-vapor interface. Different vapor structures are formed due to the interaction between near bubbles.

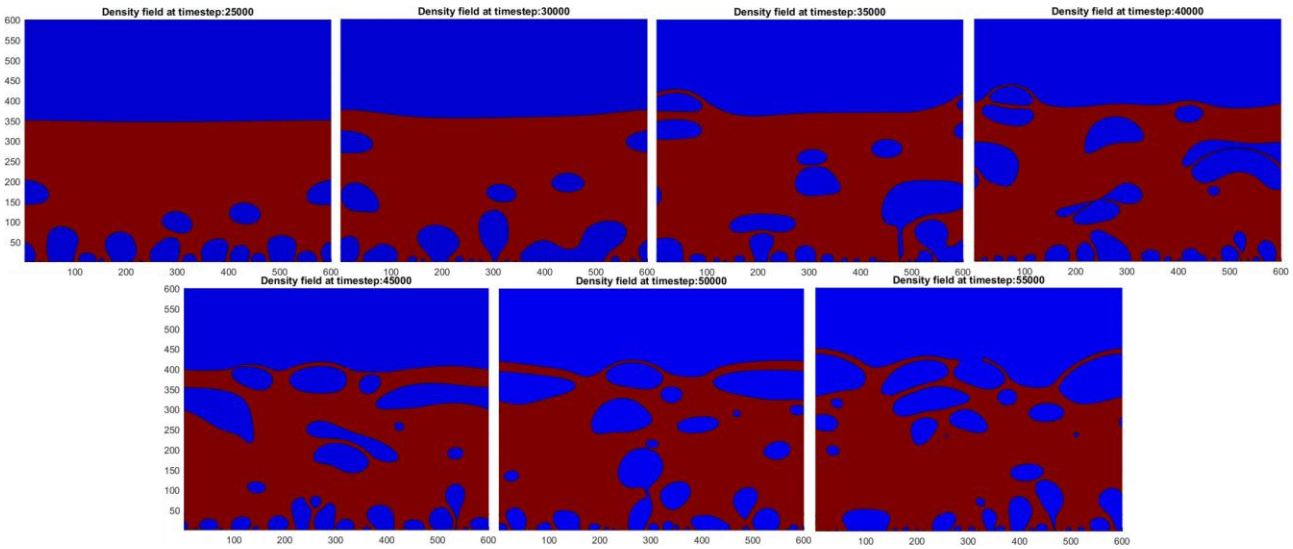

Figure 6. Snapshots of the boiling process with $G_s = 0$ and $\Delta T = 0.0248$.

In order to investigate the model capabilities to simulate the boiling process at even higher superheating degrees, this parameter is increased to $\Delta T = 0.0495$ after 20000 timesteps. The results are presented in Fig. 7. It can be noticed that the further increase in the superheating degree resulted in a vapor film covering the heated surface. This feature could be associated with film boiling regime. In this case, when the liquid reaches the heated surface, intense liquid-vapor evaporation will happen, leading to some rising bubbles in the vapor film.

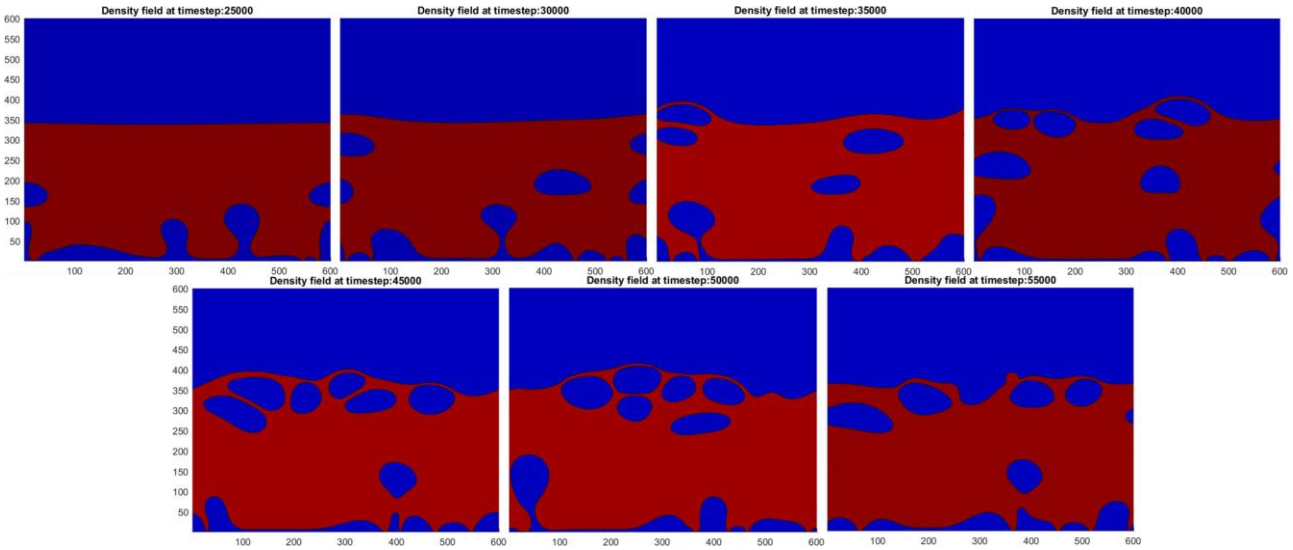

Figure 7. Snapshots of the boiling process with $G_s=0$ and $\Delta T=0.0495$.

Now, the simulations are performed with different strengths of the solid-fluid interaction, resulting in different wettability conditions. This is performed by changing the parameter G_s, in Eq. (12). Among the results presented in Fig. 5 in which $G_s = 0$, simulations are performed considering $G_s = 0.065$ and $G_s = 0.105$. In these two cases, the equilibrium contact angles are approximately equal to 50° and 55.5°, respectively. In Fig. 8 and Fig. 9 these numerical results are presented, respectively. By increasing the parameter G_s, the liquid contact angle increases and hence, the surface wettability decreases. It this case, it is expected that the vapor nuclei will spread and accumulate more in the heated

surface. This effect can be observed also comparing the results with the ones presented in Fig. 5, in which $G_s = 0$ was considered. It should be mentioned that the liquid wettability plays an important role in the boiling process, since if the liquid does not wet the heated surface accordingly, the film boiling regime is more easily achieved.

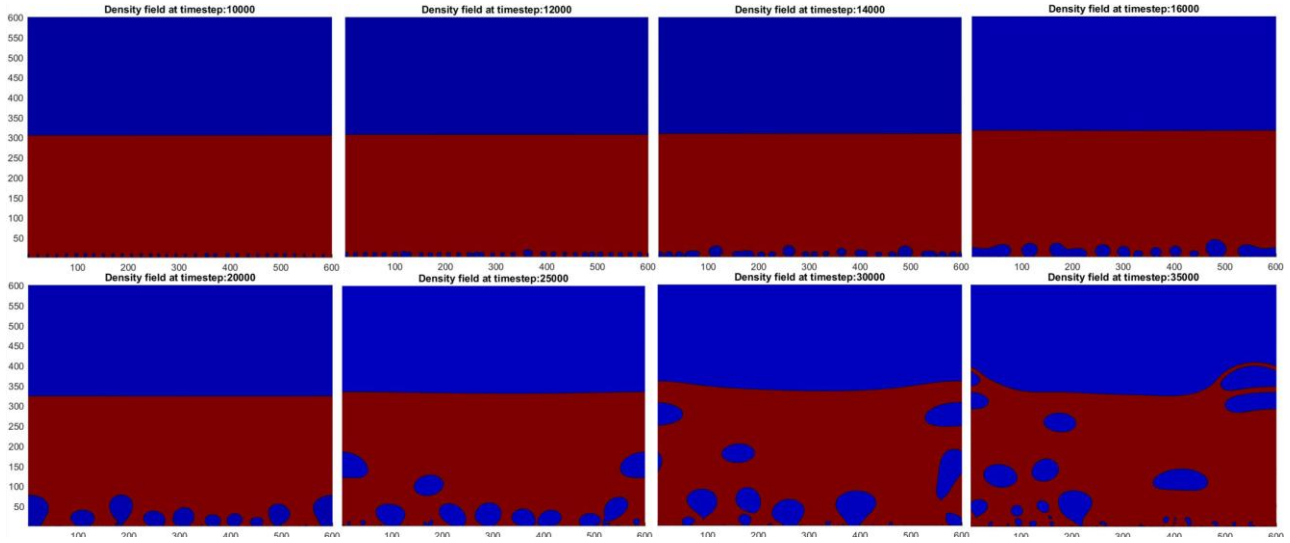

Figure 8. Snapshots of the boiling process with $G_s = 0.065$ and $\Delta T = 0.0165$.

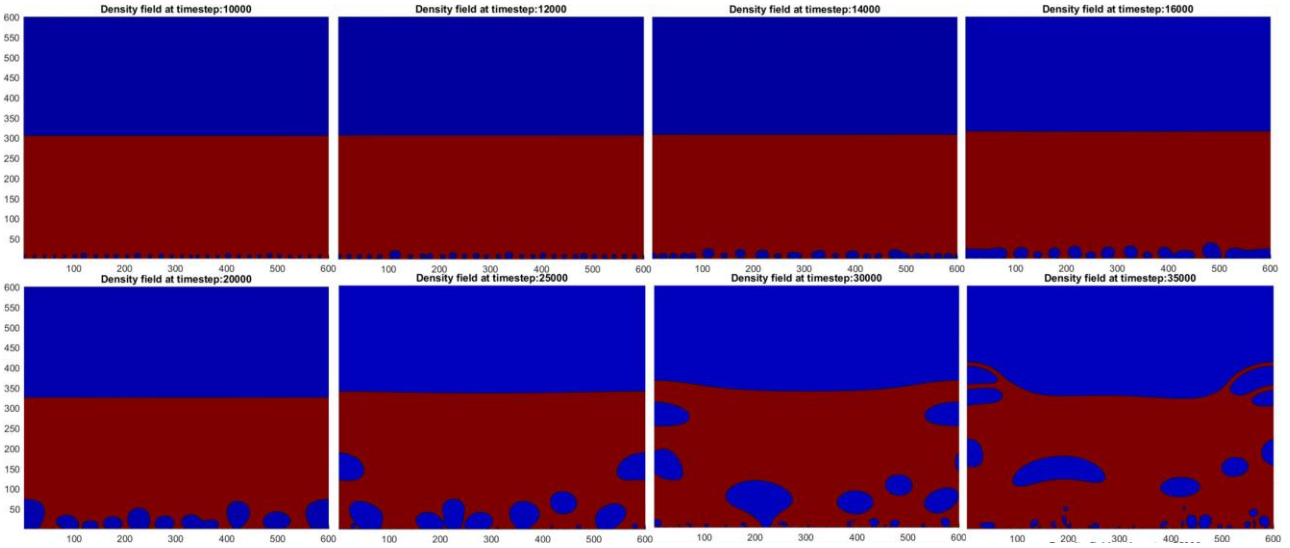

Figure 9. Snapshots of the boiling process with $G_s = 0.105$ and $\Delta T = 0.0165$.

Finally, the combined effect of low wettability with $G_s = 0.105$ and higher superheating degree, $\Delta T = 0.0495$, is analyzed. The results are presented in Fig. 10. It can be seen that due to the lower wettability, a more stable vapor film is established in the heated surface when compared with the results presented in Fig. 7. From a qualitatively analysis, the boiling regime presented in Fig. 10 can be associated with film boiling.

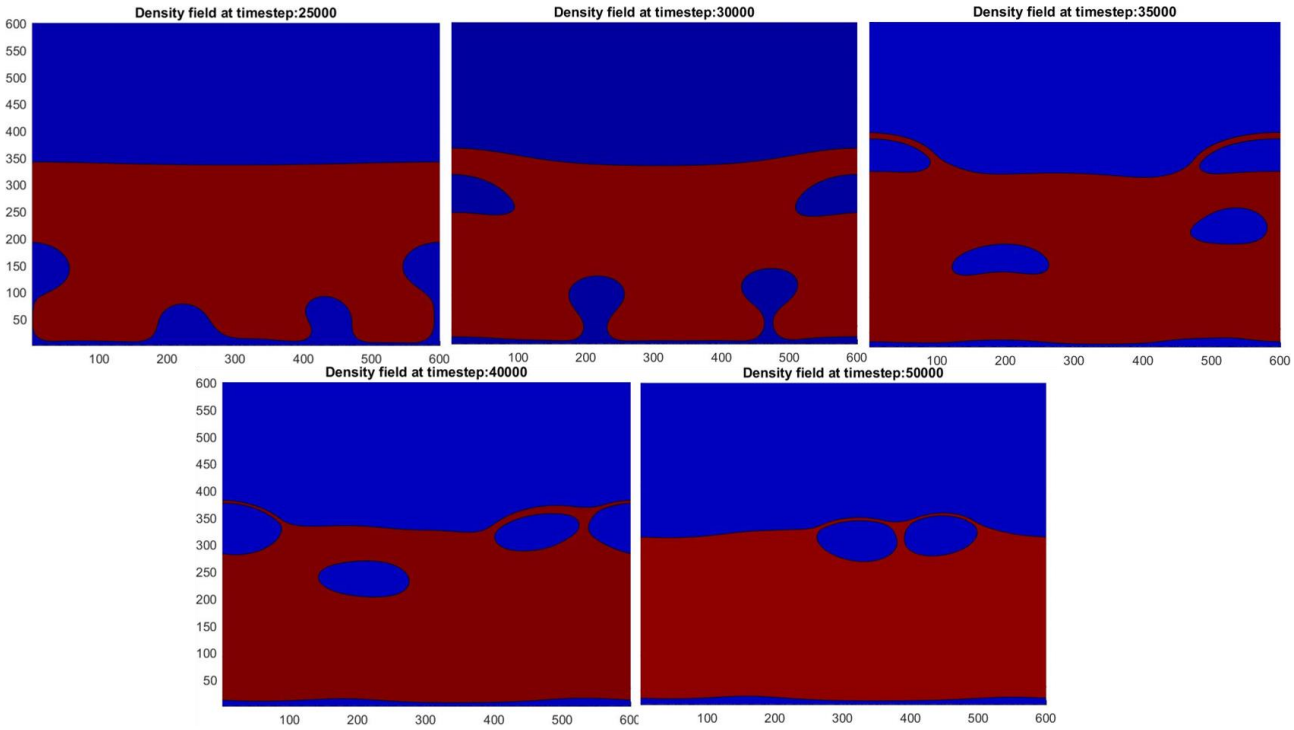

Figure 10. Snapshots of the boiling process with $G_s = 0.105$ and $\Delta T = 0.0495$.

4. CONCLUSIONS

In this paper, the methodology proposed by Li et al. (2015) for the MRT collision operator have been applied to the BGK collision operator to simulate boiling heat transfer. In this model, a hybrid pseudopotential Lattice Boltzmann Method have been considered for the simulations. The density and velocity fields were obtained from a distribution function and the temperature field was obtained from the solution of a macroscopic energy conservation equation using a traditional 4th order Runge-Kutta scheme.

First, numerical simulations of bubble nucleation, growth and departure were presented. A comparison between the numerical results of bubble departure diameter and release period with theoretical relations was performed. Good agreement between numerical and theoretical results was found.

Later, the model was applied to simulate boiling heat transfer. A qualitative analysis was performed considering different liquid wettability and superheating degree. The results showed that higher superheating degree will enhance bubble nucleation, as expected. The model was able to reproduce qualitative results of nucleate and film boiling, respectively. The liquid wettability was analyzed by tuning a surface parameter. The model allowed the variation of wettability to simulate boiling heat transfer, producing physically consistent results.

Future analysis will be performed with this numerical model, including a comparison against experimental data from the literature. Also, the model will be extended to perform three dimensional simulations of boiling heat transfer.

ACKNOWLEDGMENTS

The authors acknowledge the support received from FAPESP (Processes 2016/09509-1; 2018/09041-5) and CNPq (Processes 431782/2018-0; 304972/2017-7).

5. REFERENCES

Anderson, D. M., McFadden G. B., Wheeler, A. A., 1998. "Diffuse-interface methods in fluid mechanics". *Annual Review of Fluid Mechanics*, Vol. 30, pp. 139-165.

Atkinson, K.E. An Introduction to Numerical Analysis, second ed., John Wiley & Sons, New York, 1989.

Chen, H., Chen, S., Matthaeus, W.H., 1992. "Recovery of the Navier–Stokes equations using a lattice-gas Boltzmann method". *Physical Review E*, Vol. 45, pp. 1 – 4.

Fritz, W., 1935. “Berechnung des maximalen Volumens von Dampfblasen”. *Physik. Zeitschr*, Vol. 36, pp. 379-384.

Gong, S. and Cheng, P., 2012. "A lattice Boltzmann method for simulation of liquid–vapor phase-change heat transfer". *International Journal of Heat and Mass Transfer*, Vol. 55, pp. 4923–4927.

Gong, S. and Cheng, P., 2015a. "Lattice Boltzmann simulations for surface wettability effects in saturated pool boiling heat transfer". *International Journal of Heat and Mass Transfer*, Vol. 85, pp. 635-646.

Gong, S. and Cheng, P., 2015b. "A lattice Boltzmann method for simulation of liquid–vapor phase-change heat transfer". *International Journal of Heat and Mass Transfer*, Vol. 80, pp. 206–216.

Guo, Z., Zheng, C., Shi, B., 2002. "Discrete lattice effects on the forcing term in the lattice Boltzmann method". *Physical Review E*, Vol. 65, pp. 046308-1–046308-6.

Hazi, G. and Markus, A., 2009. "On the bubble departure diameter and release period based on numerical simulation results". *International Journal of Heat and Mass Transfer*, Vol. 52, pp. 1472–1480.

Li, Q., Kang, Q.J., Francois, M.M., He, Y.L., Luo, K.H., 2015. "Lattice Boltzmann modeling of boiling heat transfer: The boiling curve and the effects of wettability". *International Journal of Heat and Mass Transfer*, Vol. 85, pp. 787–796.

Li, Q., Zhou, P., Yan, H.J., 2017. "Improved thermal lattice Boltzmann model for simulation of liquid-vapor phase change". *Physical Review E*, Vol. 96, pp. 063303.

Shan, X. and Chen, H., 1993. "Lattice Boltzmann model for simulating flows with multiple phases and components". *Physical Review E*, Vol. 47, pp. 1815–1819.

Shan, X. and Chen, H., 1994. "Simulation of nonideal gases and liquid-gas phase transitions by the lattice Boltzmann equation". *Physical Review E*, Vol. 49, pp. 2941–2948.

Zhang, R. and Chen, H., 2003. "Lattice Boltzmann method for simulations of liquid-vapor thermal flows". *Physical Review E*, Vol. 67, pp. 066711-1–066711-6.

Zou, Q. and He, X., 1997. "On pressure and velocity boundary conditions for the lattice Boltzmann BGK model". *Physics of Fluids*, Vol. 9, pp. 1591–1598.

Zuber, N., 1963. "Nucleate boiling. The region of isolated bubbles and the similarity with natural convection". *International Journal of Heat and Mass Transfer*, Vol. 6, pp. 53–78.

6. RESPONSIBILITY NOTICE

The authors are the only responsible for the printed material included in this paper.